



OPEN Thermal stability assessment of calcium monosulfoaluminate 12-hydrate by applying the in-situ X-ray diffraction method at 25–1250 °C

Dovile Rubinaite^{1✉}, Tadas Dambrauskas¹, Kestutis Baltakys¹, Harald Hilbig² & Raimundas Siauciunas¹

In this study, the stability of synthetic calcium monosulfoaluminate and the reaction mechanism of its conversion into ye'elimite during the thermal treatment were examined. The monosulfoaluminate was produced referring to ye'elimite stoichiometry by applying the mechanochemical treatment (dry grinding at 900 rpm with 3 on–off cycles of 10 min) followed by the hydrothermal synthesis (for 8 h at 110 °C). The data indicated that the prepared sample consists of Ms12 (~ 54.8%), CaCO₃ (~ 1.9%), Ms10.5/Hc (~ 0.7%) and amorphous content (~ 42.6%). Meanwhile, the thermal stability assessment by in-situ XRD analysis reveals that the dehydration of monosulfoaluminate interlayer water proceeds at 25–370 °C, where four different hydration states of monosulfoaluminate are identified. Additionally, the results suggest that the removal of water molecules from the main (octahedral) layers begins at ~ 200 °C. Finally, at 700–1250 °C, the solid-state reactions between C₄S, CA and CaO are observed, generating the formation of ye'elimite.

It is recognised that in the CaO–Al₂O₃–CaSO₄–H₂O system, two main existing phases, AFt (ettringite) and AFm (monosulfoaluminate), can be distinguished. These phases mainly form during the hydration of Portland cement and calcium sulfoaluminate/aluminate-containing binders^{1–3}. Both ettringite (C₆A₃H₃₂) and monosulfoaluminate (C₄A₁SH₁₂) precipitate from lime, aluminium and calcium sulphate solutions. In the case of ettringite formation, a sufficient amount of additional calcium sulphate is needed^{4,5}. Meanwhile, the deficiency of calcium sulphates results in the formation of monosulfoaluminate (C₄A₁SH₁₂). In addition, ettringite can convert to monosulfoaluminate when sulphate is consumed and vice versa^{1,6}.

Regarding the stability of these phases, it is essential to comprehend their behaviour in given conditions for concrete sustainability and durability. To date, the stability of these phases has been the subject of numerous studies that have raised many discussions and controversies. It is acknowledged that the stability of these phases highly depends on environmental conditions such as temperature, pressure, and relative humidity^{7,8}. However, regarding the thermal stability of monosulfoaluminate, it is not as extensively examined as ettringite^{9–12}. The main reason for this is the complexity of synthesising the pure hydration states of monosulfoaluminate and difficulties in experimental characterisation caused by their poor crystallinity. Thus, there are still some serious questions about the mechanism and reaction kinetics of monosulfoaluminate degradation that have not been thoroughly answered.

Fundamentally AFm phases are hydrated tetracalcium aluminate-ferrite minerals belonging to the layered double hydroxide family (LDH-type)¹³. The structure consists of positively charged main layers [Ca₂(Al,Fe)(OH)₁₂]⁺, which are compensated by negatively charged interlayers [X·nH₂O]. Particularly this paper focuses on the aluminium AFm phase containing sulfate (SO₄²⁻) anions, identified as calcium monosulfoaluminate 12-hydrate (monosulfate or monosulfoaluminate). As mentioned before, it is a prevailing compound in cement hydrate systems and has the naturally occurring structure analogue – mineral Kuzelite (C₄A₁SH₁₂), as was characterised by Allmann¹⁴. The essential feature of the monosulfoaluminate structure is that the water content of

¹Department of Silicate Technology, Kaunas University of Technology, Radvilenu pl 19, LT – 50254 Kaunas, Lithuania. ²Professorship for Mineral Construction Materials, TUM School of Engineering and Design, Technical University of Munich, Franz-Langinger-Str. 10, 81245 Munich, Germany. ✉email: dovile.rubinaite@ktu.lt

interlayers may alter from 2 to 10 molecules, depending on the exposure to temperature and relative humidity¹⁵. Therefore, different hydration states of monosulfoaluminate are commonly denoted by an abbreviation followed by an index indicating the water content in the interlayer. This denotation has also been used in this work; for instance, calcium monosulfoaluminate 12-hydrate is denoted as Ms12.

Despite the difficulties of producing monosulfoaluminate, it can be synthesised by applying various methods. The first synthesis of monosulfoaluminate was reported by H. J. Kuzel in 1965¹⁶. The lab-scale production process was performed using a stoichiometric mixture of tricalcium aluminate (C_3A) and gypsum ($CaSO_4 \cdot 2H_2O$), applying hydrothermal treatment at 150 °C for 4 days. In comparison, scientists have also synthesised monosulfoaluminate using the thermal decomposition (commonly at ~114 °C) method on ettringite¹⁷. However, the drawbacks of this process include the complexity of synthesis and the occurrence of calcium sulphate in the final products. Nowadays, C_3A and gypsum (suspended in a 1:1 molar mixture) are commonly used as precursors for the synthesis when the prepared suspension is stirred periodically for two weeks at 80 °C^{15,18}.

The phenomenon of multiple transformations accompanied by mass change during the thermal decomposition of calcium monosulfoaluminate has already been successfully observed in multiply works. The decomposition/dehydration process of monosulfoaluminate has been extensively studied by H. Pöllmann (1984)¹⁹. He has reported that the loss of the six interlayer water molecules proceeds between 43 and 200 °C. Meanwhile, the six remaining water molecules from the main layers are lost between 200 and 300 °C. Other authors have suggested that the crystalline water from the octahedral layer is lost in slightly higher temperatures (250–300 °C)^{20–22}. Accordingly, the remaining mass loss beyond this temperature is associated with the dehydration of the main layers. However, most of the previous studies dealing with the stability of monosulfoaluminate were mainly validated by thermal analysis (DSC/TG) and ex-situ XRD experimental results. These results do not demonstrate the precise mechanism and kinetics of degradation reactions of monosulfoaluminate, leaving not well-resolved questions about the decomposition of monosulfoaluminate.

High-temperature X-ray in-situ analysis is a powerful tool that allows real-time observations of phases transition and assists in revealing the reaction mechanism²³. Additionally, this method enables the detection of intermediate phases in reactions or high-temperature phases that recrystallise to low-temperature phases during the cooling processes. The features of this method are essential for the correct study of the phase transitions of different hydration states of monosulfoaluminate since the ambient conditions significantly affect their stability. Only a few scientists have attempted to apply in-situ method measurements to investigate its stability. N. Meller has presented the hydrothermal decomposition of calcium monosulfoaluminate 14-hydrate by applying the in-situ synchrotron X-ray diffraction method¹⁷. Meanwhile, H. Pöllmann characterised the stability of kuzelite by in-situ X-ray investigation²⁴. Nevertheless, none of the protocols describes detailed experimental conditions; one piece of information is always missing. In addition, there is a lack of elaboration on the obtained results, such as the beginning and end temperatures of the phases' transition. Therefore, the answers to open-ended questions such as the stability of calcium monosulfoaluminate remain obscure.

Thus, synthetic calcium monosulfoaluminate dehydration sequences and the formation of crystalline phases mechanism at elevated temperatures are highlighted in this study. For the synthesis of calcium monosulfoaluminate, the mechanochemical-hydrothermal treatment approach was used. Meanwhile, the thermal stability was investigated by applying the in-situ XRD method and complemented with simultaneous thermal analysis. Finally, the results provide new insights into the mechanism behind the observed dehydration of calcium monosulfoaluminate.

Materials and methods

Raw materials. For the synthesis of calcium monosulfoaluminate, reagent-grade materials were used:

- Calcium carbonate ($CaCO_3$, *Eksparas*, Lithuania), with purity ≥ 99.0 wt.% of $CaCO_3$;
- Aluminium hydroxide ($Al(OH)_3$, *Honeywell*, Germany) with purity ≥ 99.0 wt.% of $Al(OH)_3$;
- Gypsum ($CaSO_4 \cdot 2H_2O$, *Lach-Ner*, Poland), which consisted of 27.07 wt.% of Ca, 20.64 wt.% of S, and other substances (up to ~1% wt.%).

The composition of the initial mixture was prepared based on ye'elimite ($Ca_4Al_6O_{12}(SO_4)$) stoichiometry. Calcium oxide (CaO) was obtained from calcium carbonate calcinated at 950 °C temperature for 1 h (the loss on ignition ~42.9%), where the quantity of free CaO was equal to ~98.2 wt.%. Meanwhile, the aluminium oxide (Al_2O_3) was prepared by dehydration of aluminium hydroxide at 475 °C temperature for 4 h (the loss on ignition ~34.2%). Both mentioned substances were sintered in an electric muffle furnace *SNOL 8.2/1100* (Umega group, AB, Lithuania).

Synthesis process. Synthesis of calcium monosulfoaluminate was performed by applying the mechanochemical treatment and hydrothermal synthesis. In the first stage, the mechanical treatment of the initial mixture was performed using a high-energy vibrating cup mill *Pulverisette 9*. The grinding operated at 900 rpm with three on-off cycles of 10 min. It was observed that the mechanochemical treatment causes great structure and phase composition changes in the initial mixture. It was confirmed by XRD measurements performed before and after grinding for different durations (Fig. 1).

The results show that within the first 10 min of milling, the mechanochemical treatment induces dehydration of gypsum, i.e., a significant decrease in the diffraction peaks characteristic of gypsum ($CaSO_4 \cdot 2H_2O$, PDF No. 04-010-9409) is observed²⁵. Additionally, due to partial water evaporation out of the gypsum structure, bassanite ($CaSO_4 \cdot 0.5H_2O$, PDF No. 00-033-0310) is detected in the XRD patterns. At the same time, prepared calcium oxide (CaO, PDF No. 00-037-1497) reacts with water resulting in the formation of portlandite ($Ca(OH)_2$, PDF

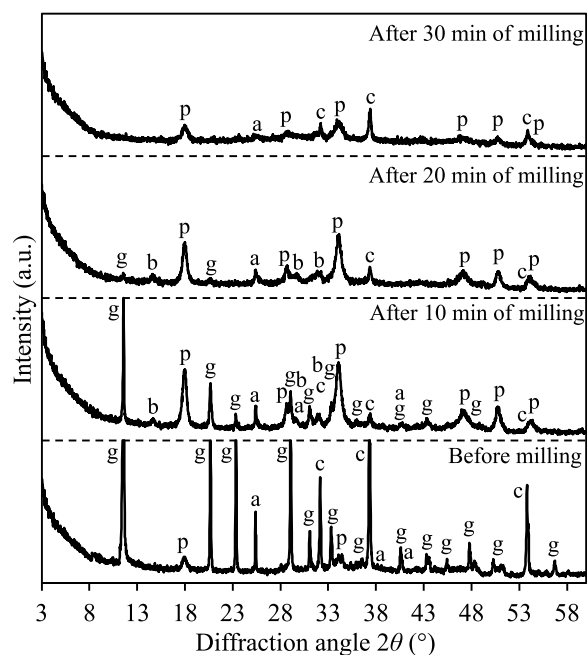


Figure 1. XRD patterns of the initial mixture at the different stages of mechanochemical treatment. The X-rays with a wavelength of 1.5406 Å (CuK α radiation) were used. Indexes: g – gypsum, p – portlandite, c – calcium oxide, a – anhydrite, b – bassanite.

No. 00-044-1481). Meanwhile, mechanochemical milling induces damage in the crystalline structure of anhydrite (present from the raw material) (CaSO₄, PDF No. 00-037-1496), causing its reflections of diffraction peaks to reduce. This tendency is seen with further milling (up to 30 min) for almost all diffraction peaks of compounds of the initial mixture. It is evident that mechanochemical treatment induces the disintegration of the structure of the crystalline phases. The exception is observed only for calcium oxide, which reflections increase with increasing milling duration due to portlandite dehydration. It is worth mentioning that alumina exhibits an amorphous nature if it is produced by dehydration of Al(OH)₃ below 700 °C^{26,27}. Therefore, in this case, aluminium oxide is not seen in the XRD patterns. After the processing, the ground powder particle size distribution (present in Fig. 2) and density (3380 kg/m³) were measured.

In the second stage, the mechanochemical activated powder was treated in a hydrothermal environment. Firstly, the necessary amount (2 g) of powder was weighed, poured into 25 mL PTFE cells, and stirred with distilled water to reach a water/solid ratio equal to 10. The stirring was performed using a laboratory spatula for ~1 min. The hydrothermal synthesis was carried out in unstirred suspension autoclave Parr instruments 4621 (Germany). The synthesis temperature (110 °C) was reached within 2 h, and the samples were stored for 8 h. An essential part of this process was the cooling stage—The suspension must be taken out not lower than 60 °C.

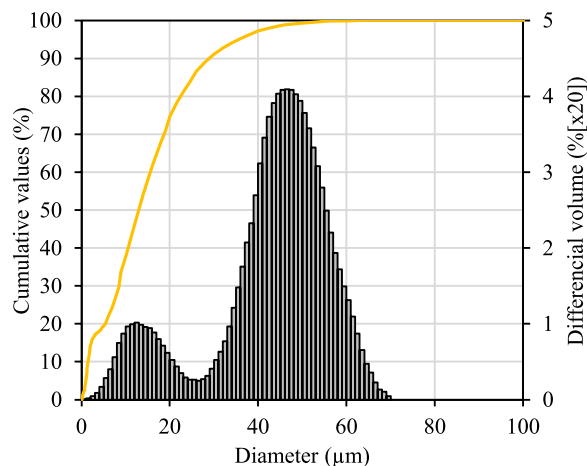


Figure 2. Particle size distribution of the ground mixture after 30 min.

It was observed that cooling down the suspension in the autoclave below 60 °C promotes ettringite formation. This observation coincides well with D. Damdot and F. P. Glasser estimations²⁸, demonstrating that above 45 °C temperature, monosulfoaluminate is significantly more stable compared to ettringite. Meanwhile, recrystallisation of monosulfoaluminate to AFt, C₃AH₆ and gibbsite is possible at lower temperatures. After hydrothermal treatment, the suspension was decanted, rinsed with acetone, and filtered. For X-ray diffraction measurement, the wet sample was used directly after filtration. Meanwhile, the dry sample was prepared by drying at 50 ± 0.2 °C for 24 h in a dryer SP-25 EASY (Kambič, Slovenia). The obtained dry samples were sieved through a sieve with a mesh width of 80 µm to ensure particle distribution.

Methods. The particle size distribution of the prepared initial mixture was analysed by °ILAS LD 1090 LD grain-size analyser (Cilas, Orleans, France), and the density was by automatic gas pycnometer *Ultrapyc 1200e* (Quantachrome Instruments (Micromeritics, USA)).

The elemental compositions of materials were analysed by the X-ray fluorescence spectroscopy (XRF) analytical technique. The analysis was performed by a Bruker X-ray S8 Tiger WD (Bruker AXS GmbH, Karlsruhe, Germany) spectrometer equipped with the Rh tube (60 keV), the measurement atmosphere – He. The analysis was carried out on samples after passing through a 63 µm sieve and then compressed (20 MPa for 45 s) into 5 × 40 mm cylindrical tablets. The obtained data were analysed with *SPECTRAPlus QUANT EXPRESS* standardless software.

The X-ray diffraction analysis (XRD) was carried out to determine the crystallographic structure of materials. The measurements were performed at room temperature with the *D8 Advance* diffractometer (Bruker AXS GmbH, Karlsruhe, Germany) equipped with a CuKα X-ray tube operated at 40 kV and 45 mA. Diffraction patterns were recorded in the Bragg–Brentano geometry using a fast-counting detector *Bruker LynxEye* based on silicon strip technology. The measurement range was $2\theta = 3\text{--}70^\circ$ with steps of $0.020^\circ 2\theta$ with the time per step 0.2 s, corresponding to a total measurement duration of ~ 12 min per sample.

The quantitative content of the crystalline phases was refined by the Rietveld method as implemented in the *TOPAS 4.2 software* (Bruker AXS GmbH, Karlsruhe, Germany). The quantitative phase analysis (QPA) was carried out on samples after grinding by hand to pass a 40 µm sieve, ensuring an isotropic distribution of the crystals in the sample. For the quantitative determination of the amorphous phase, 20% of the internal standard (ZnO) was added to the sample. Additionally, the sample holder was rotated during the data recording to improve the particle statistics and obtain high-quality QPA data. The crystal structures used in the refinements were adopted from PDF 2022 database.

The thermal stability of monosulfoaluminate was investigated by applying the XRD in-situ method with the *MTC-HIGHTEMP* chamber (Bruker AXS, Karlsruhe, Germany). The samples for the measurement were prepared by mixing the powder (~0.2 g) with ethanol (96%) until the viscous consistency was reached. Afterwards, the thin suspension layer was placed on the heating strip. The experiments were performed in the temperature range of 25–1250 °C, with 50 °C/min, in an air atmosphere. The patterns were recorded after equilibration of 2 min at the desired temperature in the range $2\theta = 8\text{--}38^\circ$ with steps of ~ 0.02° 2θ and 0.2 s counting time per step. In total, 78 patterns were recorded within ~ 11.5 h.

Simultaneous thermal analysis (STA: differential scanning calorimetry – DSC and thermogravimetry – TG) measurements of synthesis products were carried out using a *LINSEIS STA PT 1000* (Linseis Messgeraete GmbH, Selb, Germany) thermal analyser with the type S thermocouple. The sample (10 ± 0.02 mg) was heated in the temperature range of 30–950 °C at a heating rate of 5 °C/min. The analysis was performed in the standard closed Pt-10 wt. % Rh crucibles under nitrogen flow, and the measurement accuracy reached ± 3 °C. The obtained results were analysed using the *Linseis Platinum Evaluation* software. Meanwhile, the additional DSC was performed with a Netzsch Polyma DSC 214 analyser (Netzsch, Germany) with the type E thermocouple. Measurement parameters: temperature heating rate – 5 °C/min, temperature range – 15–400 °C, the crucible – aluminium (Al) crucible with a lid, the atmosphere in the furnace – nitrogen, measurement accuracy – ± 3 °C. The data were assessed with NETZSCH Proteus software.

The Fourier transform infrared spectroscopy (FTIR) analysis was carried out using the *Perkin Elmer FT-IR Spectrum X system* (PerkinElmer, Waltham, MA, USA). The samples were analysed using the KBr pressed pellet technique (~ 1 mg of sample and ~ 200 mg of KBr), and spectra were recorded in the range of 4000–400 cm⁻¹ with a spectral resolution of 1 cm⁻¹.

The morphology of the samples was investigated by scanning electron microscopy (SEM) (JEOL JSM-7600F, Japan). The micrographs were obtained using an accelerating voltage of 10 kV under a high vacuum at a working distance of 5.0 mm and 4.9 mm.

The ²⁷Al NMR spectroscopy was carried out with a *Bruker Avance 500* spectrometer (Bruker, Germany) with a magnetic field strength of 11.747 T (resonance frequency for ²⁷Al: 130.308 MHz). The measurements were performed applying a single pulse MAS (magic angle spinning) technique. The samples were placed in a 4 mm zirconia rotor and spun at 12 kHz with a repetition time of 0.5 s, recording a total of 2000 scans. The ²⁷Al chemical shifts were referenced relative to the Al(OH)₃. The obtained spectra patterns were assessed using WINNMR software.

Results and discussion

Mineralogical composition and microstructure of the hydrothermal synthesis product. In the first stage of this research, the mineralogical composition and microstructure of the hydrothermal synthesis products were investigated. In order to evaluate the drying impact on crystalline phase assemblage, wet and dry samples were used for XRD diffraction analysis. As shown in the XRD patterns in Fig. 3a, calcium monosulfoaluminate 14-hydrate (Ms14) (Ca₄Al₂O₆(SO₄)·14H₂O, PDF No. 00-042-0062) is observed as the main crystalline phase directly after the hydrothermal synthesis. Meanwhile, after the drying process (at

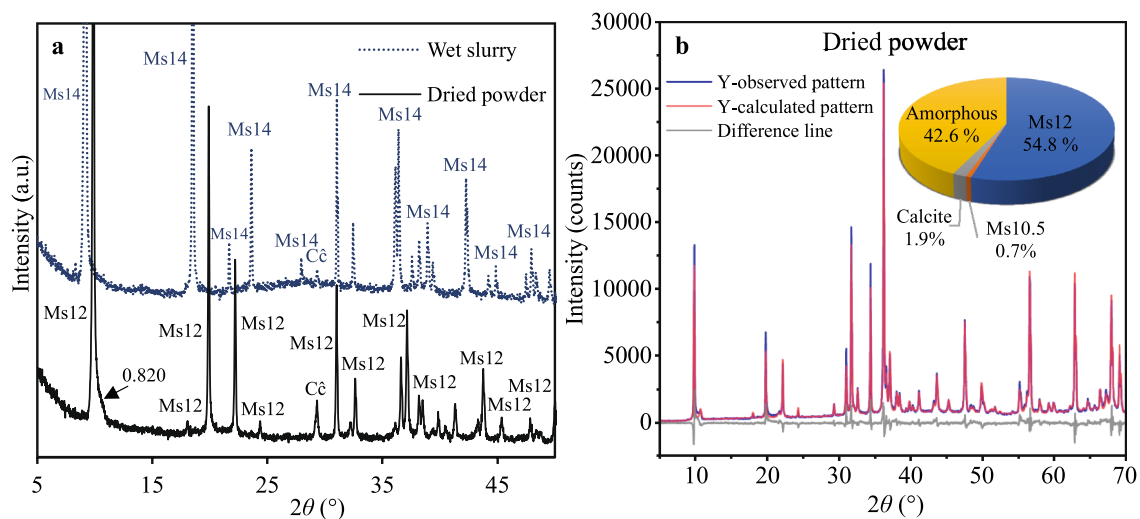


Figure 3. XRD patterns (a) and QPA results (b) of the samples after hydrothermal synthesis. The X-rays with a wavelength of 1.5406 Å (CuK α radiation) were used. Indexes: Ms – monosulfoaluminate (the number shows water content); Cc – CaCO $_3$.

50 °C for 24 h), a lower hydration state is detected, corresponding to calcium sulfoaluminate 12-hydrate (Ms12) (Ca $_2$ (SO $_4$) $_0.5$ (OH) $_6$ (H $_2$ O) $_3$, PDF No. 04-013-03303). The results clearly show that Ms14 is a transition hydrate that loses two interlayer water molecules exposed to elevated temperature and dehydrates into Ms12. In addition, calcium carbonate (CaCO $_3$, PDF No. 01-080-2793) and a small broad diffraction peak at $\sim d - 0.820$ nm are observed in the XRD patterns of dried samples. The detected broadening can be ascribed to the formation of calcium hemicarboaluminate (Hc) or calcium monosulfoaluminate 10.5-hydrate. The mentioned compounds could have been formed through Ms12 interaction with atmospheric CO $_2$ or CaCO $_3$ and/or partial Ms12 dehydration as Hc and Ms10.5, respectively¹⁸. However, the peak intensity is too low to identify the true nature of the formed phase. For further study, analysis methods were applied only to dried samples.

For the quantitative phase analysis, it was assumed that the diffraction peak at $\sim d - 0.820$ reflects the Ms10.5 structure. As the crystal structure patterns of the lower monosulfoaluminate hydration states (below Ms12) remain vague, the crystal structure of kuzelite was used as a starting model for Ms10.5 refinement. Aiming for adequate QPA data results, the space group and initial lattice parameters were adjusted considering the previous studies¹⁵. The phase composition results of the sample are presented in Fig. 3b.

The further characterisation of the sample after hydrothermal synthesis was done by FTIR spectroscopy which confirmed and supplemented the XRD analysis results. As shown in Fig. 4, two distinct regions are detected in the FTIR spectrum. The first, high-frequency region (4000–2500 cm $^{-1}$) distinctly represents the OH stretching vibrations. The band at frequencies of 3635–3637 cm $^{-1}$ indicate OH-stretching and confirms the presence of amorphous aluminium hydroxide (AH $_3$). Furthermore, the broad absorption band, recorded between 3600 and 2900 cm $^{-1}$, corresponds to the stretching vibrations of hydroxyl groups in the interlayer and the main layer of the monosulfoaluminate. Meanwhile, the second low-frequency region of the spectrum is seen below 2000 cm $^{-1}$. In this region, the interpretation of the experimental data is more complex since many overlaps of the vibrational bands are observed. The detected absorption band at 1630 cm $^{-1}$ corresponds to the bending vibration of the interlayer water molecules. Furthermore, the absorption band at 1455 cm $^{-1}$ and 875 cm $^{-1}$ shows asymmetric stretching vibration of CO $_3$, indicating the presence of calcium carbonate. Towards the lower energies (below 1200 cm $^{-1}$) are indicated absorptions of the SO $_4$ $^{2-}$ (stretching at 1109 cm $^{-1}$, bending at 423 cm $^{-1}$), Al–O–H

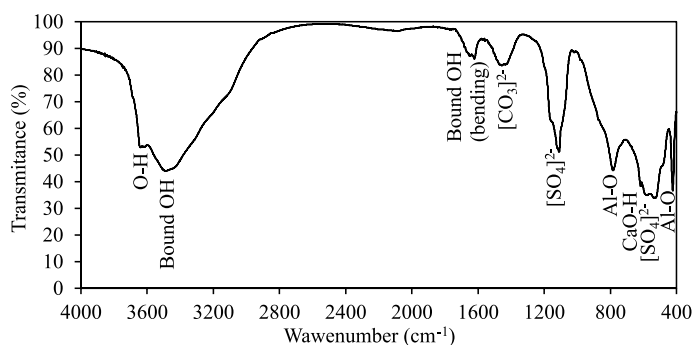


Figure 4. FTIR spectrum of the sample after hydrothermal synthesis.

(bending at 785 cm^{-1} and 617 cm^{-1}) and AlO_6 vibration (at 588 cm^{-1} , 522 cm^{-1}). The interpretation of the FTIR spectrum bands agrees well with the previously published data^{29–31}.

The ^{27}Al NMR analysis was used to examine the amorphous nature of the sample. The obtained data of the sample is presented in Fig. 5. The ^{27}Al NMR spectrum of the sample shows two resonance ranges at the higher (from 80 to 45 ppm) and lower (from 30 to -30 ppm) fields, reflecting resonances for fourfold and sixfold coordinated Al positions, respectively³². The dominant peak at ~ 9.4 ppm is a characteristic signal of AlO_6 in monosulfoaluminate. Meanwhile, a broad shoulder at ~ 67 ppm corresponds to the presence of unreacted Al_2O_3 , with the resonance of the sixfold coordinated aluminium part being hidden under the resonance of the monosulfoaluminate. According to XRD and ^{27}Al NMR results, mainly amorphous content consists of unreacted Al_2O_3 . In addition, the deconvolution demonstrates a small peak at $0\text{--}2$ ppm, indicating the presence of a small amount of AH_3 in the sample.

Further, the SEM analysis was used to identify the characteristic morphology of phases (Fig. 6). The images demonstrate that the sample contains particles of various sizes and morphologies. The most widely spread morphology is seen as a hexagonal plate as well as layered plates without defined borders, both corresponding to calcium monosulfoaluminate (size $\sim 5\text{--}20\ \mu\text{m}$)⁸. Additionally, these structures are surrounded by brighter various size irregular-shaped agglomerates reflecting the morphology of amorphous $\text{Al}_2\text{O}_3/\text{Al}(\text{OH})_3$ ^{27,32}. Due to the high quantity of amorphous Al_2O_3 and similar morphology, $\text{Al}(\text{OH})_3$ was not distinguished in SEM images.

Thermal stability. The structural changes associated with the thermal decomposition of the synthesis products were investigated by applying the in-situ X-ray diffraction method and simultaneous thermal analysis. It is worth noting that XRD patterns were recorded at the process temperature. Therefore, the thermal-induced shifts are visible for the positions of the peaks in the XRD patterns. Two main temperature intervals can be distinguished based on the results (Fig. 7). The first one (the phase decomposition interval) is seen in the temperature range of $25\text{--}800\text{ }^\circ\text{C}$, which is associated with dehydration and decarbonisation. Immediately after incrementing temperature, the intensity of peaks corresponding to Ms12 (main peak at $d = 0.893\text{ nm}$) begins to decrease, reflecting Ms12 dehydration. Meanwhile, the Ms12 completely dehydrates at $\sim 90\text{ }^\circ\text{C}$. At the same time, the for-

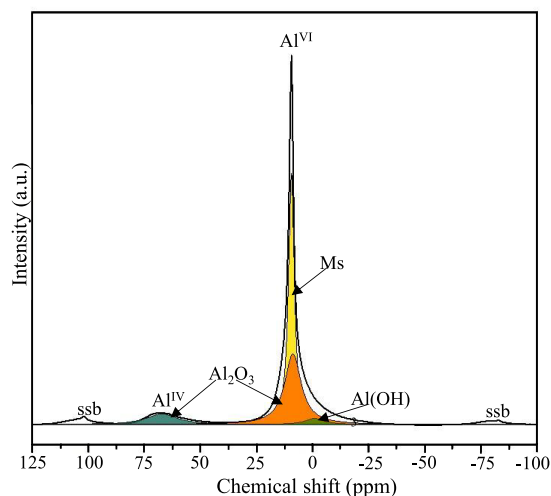


Figure 5. ^{27}Al NMR spectrum of the sample after hydrothermal synthesis.

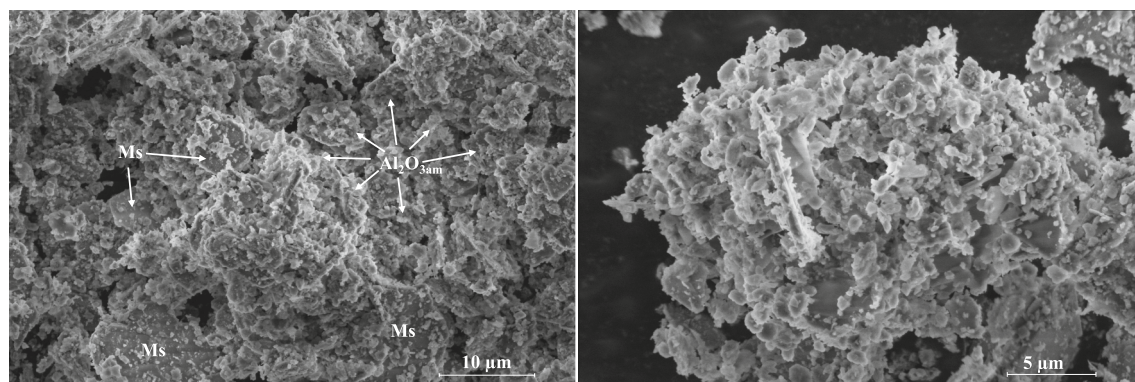


Figure 6. SEM micrographs of the sample after hydrothermal synthesis.

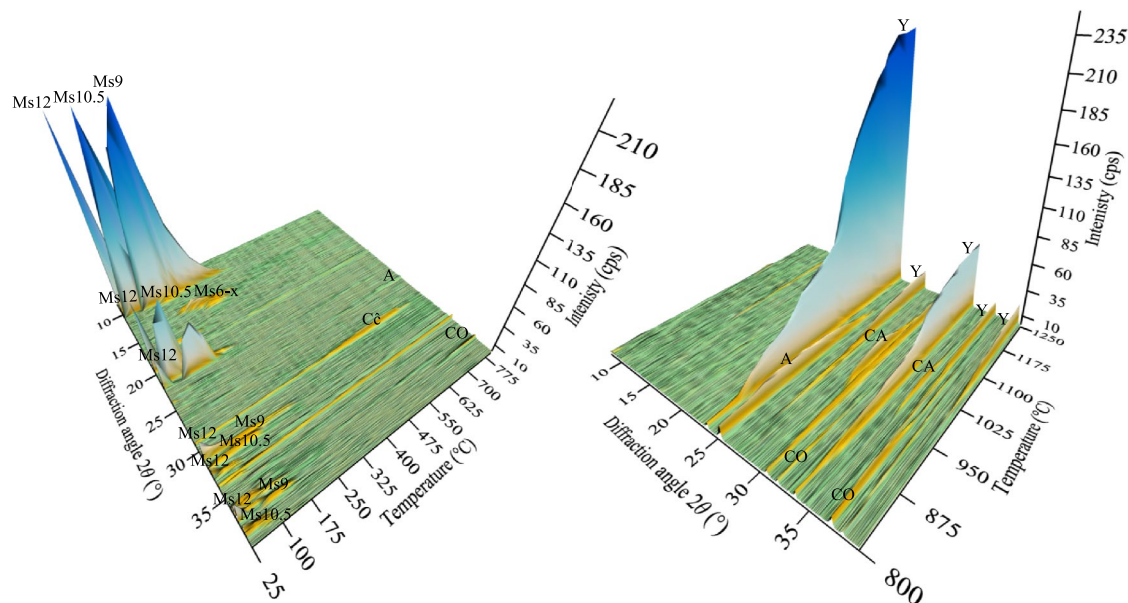


Figure 7. In situ XRD patterns of the synthesis products when the calcination temperature varied in a 25–1250 °C range. The X-rays with a wavelength of 1.5406 Å (CuK α radiation) were used. Indexes: Ms – monosulfoaluminate (the number shows water content); C \hat{c} – calcium carbonate; CO – calcium oxide; A – anhydrite; CA – calcium aluminate; Y – ye’elimite.

mation of Ms10.5 ($d = 0.814$ nm) at ~ 50 °C is observed, generated by the dehydration of Ms12. The increase in the intensity of Ms10.5 peaks is seen up to ~ 80 °C. Meanwhile, further temperature increase adversely affects the stability of Ms10.5, causing a gradual decrease in the intensity of peaks that are no longer visible at 220 °C. Similarly, the formation of a lower hydration state is observed at 90 °C, corresponding to Ms9 ($d = 0.796$ nm). The highest intensities of its peaks are seen at ~ 140 °C, while peaks remain visible even up to ~ 370 °C. These results indicate that the dehydration of Ms10.5 presumably begins at ~ 80 °C, causing the formation of Ms9. In the same way, the dehydration of Ms9 presumably begins at around ~ 140 °C, yielding the appearance of lower hydration states of monosulfoaluminate. As a result, a broad low-intensity diffraction peak at $d = 0.617$ nm is observed at 170–330 °C. Unfortunately, based on the PDF-4 database, the detected peak could not be determined. Nevertheless, this peak might indicate the transitional Ms6-x phase (x is water molecules, might be from 0 to 6), most likely it is Ms6, which may have an amorphous/low crystallinity nature. However, a high amount of formed compound and/or elevated ambient temperatures might have contributed to the peak detection. Additionally, the temperature (~ 200 °C) at which the peak intensity begins to decrease might show the beginning of the water elimination out of Ms main (octahedral) layers.

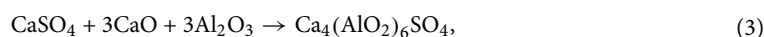
It is important to emphasise that only the main peak positions of the lower monosulfoaluminate states (Ms10.5 and Ms9) were presented in the previous studies^{15,18}. Therefore, in this work, the unclear Ms positions were assigned based on the main phase peak thermal stability. For instance, the main Ms10.5 peak is detected at 50 °C and remains visible up to 220 °C. According to this tendency, appeared and maintained peaks at this temperature interval were assigned to this hydrate state. The identified thermal stability of monosulfoaluminate states and assigned peak positions are summarised in Table 1.

Further investigation has demonstrated that no mineralogical changes arise between ~ 380 and ~ 700 °C. Meanwhile, at the end of the phase decomposition interval (at ~ 720 °C), the calcination of CaCO₃ is seen, which lasts up to ~ 800 °C. Accordingly, the peaks of calcium oxide arise ($d = 0.278$ nm) (CaCO₃ \rightarrow CaO + CO₂), which maximum intensities are seen at 940 °C. At the same time, above ~ 700 °C, the peaks of anhydrite (CaSO₄) ($d = 0.349$ nm) are detected, indicating the beginning of the crystalline phase formation interval (700–1250 °C). These observations demonstrate that the first and the second temperature intervals slightly overlap. Additionally,

Phase	Stable in the temperature interval	Interplanar distance (this work), nm
C ₄ A \hat{S} H ₁₂	25 °C < T < 90 °C	0.893; 0.490; 0.447; 0.399; 0.365; 0.288; 0.278; 0.274; 0.245; 0.241; 0.236; 0.233
C ₄ A \hat{S} H _{10.5}	50 °C < T < 220 °C	0.816; 0.481; 0.471; 0.408; 0.375; 0.357; 0.287; 0.279; 0.271; 0.243; 0.234
C ₄ A \hat{S} H ₉	90 °C < T < 370 °C	0.798; 0.492; 0.433; 0.398; 0.286; 0.280; 0.257; 0.248; 0.240
C ₄ A \hat{S} H _{6-x}	170 °C < T < 330 °C	0.616

Table 1. Thermal stability of different hydration states of calcium monosulfoaluminate states.

the appearance of CaSO_4 may mainly be attributed to the decomposition of calcium monosulfoaluminate, as shown in Eq. (1).



As the heating temperature rises to $\sim 860^\circ\text{C}$, diffraction peaks attributed to ye'elimite ($\text{C}_4\text{A}_3\hat{\text{S}}$) ($d = 0.375\text{ nm}$) begin to appear, which gradually increase with the increasing heating temperature (up to 1250°C). Simultaneously, peaks corresponding to the calcium aluminate phase (CA) ($d = 0.297\text{ nm}$) begin to appear at $\sim 940^\circ\text{C}$ (Eq. (2)). However, with the temperature rise up to $\sim 1100^\circ\text{C}$, the diffraction maximums of $\text{C}\hat{\text{S}}$, CA and CaO strongly attenuate, while those of ye'elimite are generated. This indicates that mentioned phases are consumed for the formation of ye'elimite through the solid-state reactions (Eqs. (3), (4)), and an increase in temperature promotes the interaction of the phases. It was observed that the critical temperature for CaSO_4 and CA are at 1160°C and 1200°C , respectively. Exceeding these temperatures, the previously mentioned phases are no longer recorded in the XRD patterns. In the highest thermal treatment temperature (1250°C), ye'elimite is observed as the dominating crystalline phase. Additionally, the small intensity peaks attributed to CaO also remain visible, showing incomplete solid-state reactions.

In order to obtain more information about calcium monosulfoaluminate decomposition, simultaneous thermal analysis was performed. The thermal phase transitions that occurred during the sample heating are presented in Fig. 8.

According to obtained TG/DTG/DSC results, the thermal decomposition of the sample can be divided into 5 mass loss regions. The first region of the DSC curve reflects 4 endothermic peaks (at $\sim 64^\circ\text{C}$, $\sim 82^\circ\text{C}$, $\sim 95^\circ\text{C}$ and $\sim 112^\circ\text{C}$), representing several chemical reactions that gradually took place. In comparison, only 3 effects incidents are seen in the DTG curve. Striving to ensure that the observed fourth peak in the curve is not an equipment noise, DSC measurements were carried out with another device (Netzsch Polyma DSC 214). Both devices confirmed the presence of a peak at $\sim 95^\circ\text{C}$ in the DSC curves, which might reflect crystal structure changes of monosulfoaluminate since it is not observed in the DTG case. However, further research is needed to confirm it. Nevertheless, these effects can be assigned to the removal of adsorption water, the dehydration of the amorphous compound structure, and the release of the unbonded and loosely bonded water molecules in the interlayer of the calcium monosulfoaluminate structure. This observation corresponds well with the results of XRD in-situ analysis, which demonstrated the overlapping dehydration mechanism of different hydrate states of calcium monosulfoaluminate ($\text{Ms}_{12} \rightarrow \text{Ms}_{10.5} \rightarrow \text{Ms}_9$) in this temperature interval.

The second temperature region has the highest mass loss ($140\text{--}220^\circ\text{C}$), and the effect at 168°C corresponds to the continuation of the dehydration of the interlayer water (mainly transition of $\text{Ms}_{10.5} \rightarrow \text{Ms}_9$). Based on the XRD insights, it might be argued that dehydration of the main layers begins at the end of this temperature range. Meanwhile, the dehydration behaviour between 220 and 370°C reflects not only the water loss from the main layers but also the remaining water loss out of the interlayers, i.e. dehydration of Ms_9 and lower states. Additionally, at this temperature range, the Ms thermal effect overlaps with the amorphous AH_3 thermal transition ($230\text{--}300^\circ\text{C}$)³³. In the fourth region ($370\text{--}600^\circ\text{C}$), neither DSC nor DTG reflects any thermal transition.

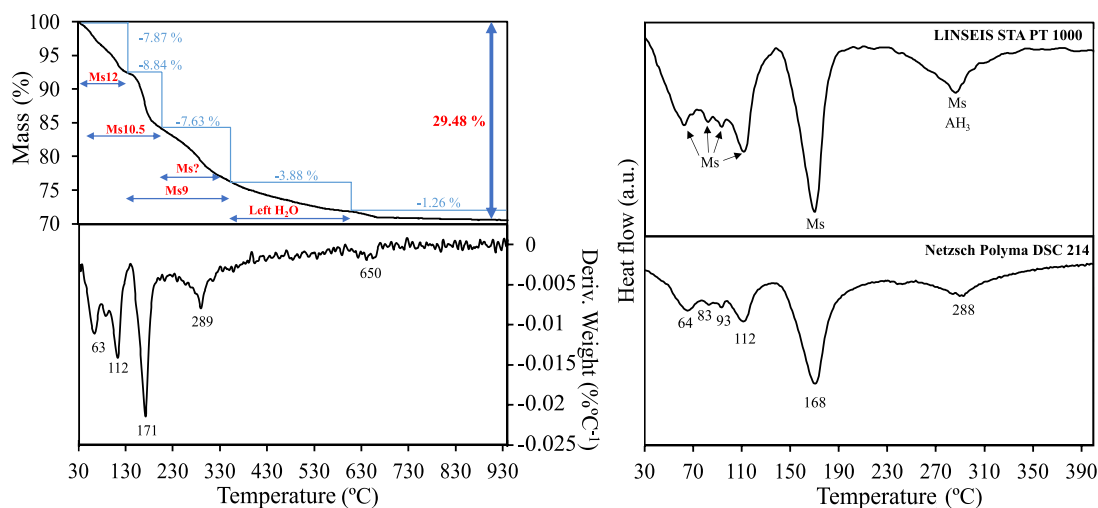


Figure 8. TG, DTG and DSC curves of the sample after hydrothermal synthesis.

However, a gradual mass loss increase in the TG curve indicates the dehydration of remaining crystal water out of Ms main layers. In the last region, the thermal shoulder (~ 650 °C) corresponds to the decomposition of CaCO_3 .

Insights of the work. The data of the current study complements the missing gaps in the thermal deterioration reaction sequences of calcium monosulfoaluminate and conversion into ye'elimite. The ranges of intermediate phases developing in the thermal heating process at 25–1250 °C are summarised and presented in Fig. 9.

As evident from the experimental data presented above, the dehydration of monosulfoaluminate occurs in a wide temperature range. The complexity of its structure (the presence of different amounts of water in the interlayers) causes the dehydration of four different hydration states of monosulfoaluminate (25–370 °C), which has been observed by in-situ X-ray diffraction. Additionally, the dehydration processes of different hydrate states of monosulfoaluminate do not take place sequentially (stepwise) but overlap. Accordingly, these results have also been confirmed by simultaneous thermal analysis: (1) the loss of mass is controlled by the removal of water from the interlayer structure and occurs in several steps, while (2) the observed water loss in the TG has poorly defined steps, that indicates the overlaps. Furthermore, this dehydration process distorted and disintegrated the crystalline structure of monosulfoaluminate, inducing the amorphization of the dehydration products. Therefore, this is the fundamental reason for limiting the application of X-ray diffraction in distinguishing the beginning and end temperatures of monosulfoaluminate main layers dehydration. Thus, further investigations are required to identify the exact dehydration temperature range of the main layers.

Meanwhile, the observation of solid-state reactions at elevated temperatures corresponds well with Y. El Khessami et al. examinations³⁴, disclosing similar mechanisms of ye'elimite formation. In contrast, the onset of ye'elimite formation is observed at a lower temperature (860 °C) compared to the conventional ye'elimite synthesis method (1000 °C). Additionally, to the best of our knowledge, the in-situ X-ray diffraction approach to observe the rapid evolution of the microstructure during ye'elimite formation has not been previously published.

It should also be considered that results show the influence of drying conditions on crystalline cement hydrate at elevated temperatures. For instance, 50 °C can condition partial dehydration and shrinkage of monosulfoaluminate (Ms12 \rightarrow Ms10.5 decrease $\sim 9\%$ in volume)¹⁵. In the long term, this can be a reason for concrete structures to deteriorate and adversely affect durability. Additionally, the temperature is essential for applying the drying techniques for sample preparation before characterising hydrated cement paste. Incorrectly chosen drying temperature can lead to the formation of different hydration states of monosulfoaluminate. Therefore, temperature and humidity must always be considered for adequate and comparable results.

Finally, it is important to underline that the identified stability ranges for different phases can be influenced and slightly altered by numerous changeable factors. Namely, grain size, degree of raw meal homogenisation, presence of impurities, experimental methods, etc. Therefore, it should be considered that the presented decomposition of monosulfoaluminate results might slightly differ in the conditions of real cementitious systems.

Conclusions

The results of the present study demonstrate the reaction sequence by which calcium monosulfoaluminate 12-hydrate dehydrates at elevated temperature and, through solid-state reactions, converts into ye'elimite. The mechanochemical treatment (dry grinding at 900 rpm with 3 on–off cycles of 10 min) followed by the hydrothermal synthesis (for 8 h at 110 °C) was applied to produce monosulfoaluminate. The ye'elimite stoichiometry was used as a reference to prepare the initial mixture from pure raw materials (CaO , Al_2O_3 , $\text{CaSO}_4 \cdot 2\text{H}_2\text{O}$).

The X-ray diffraction results show that Ms14 is the dominant crystalline phase in the synthesis products immediately after hydrothermal treatment. However, after the drying process (50 °C 24 h), Ms14 loses two

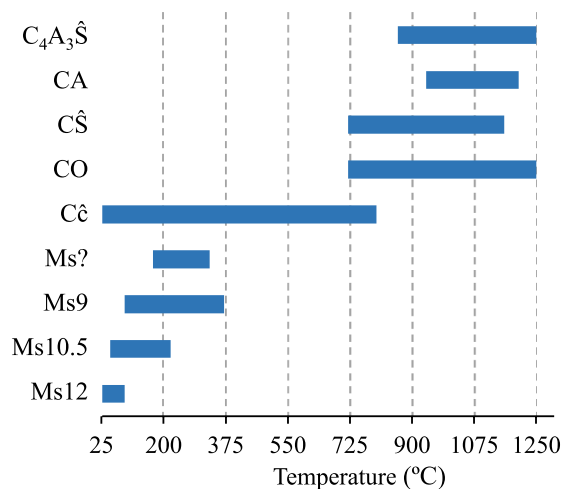


Figure 9. The ranges of crystalline phases developing in the thermal heating process of the synthesised sample detected by in-situ X-ray diffraction. Indexes: Ms – monosulfoaluminate (the number shows water content); $\hat{\text{C}}$ – calcium carbonate; CO – calcium oxide; A – anhydrite; CA – calcium aluminate; Y – ye'elimite.

interlayer water molecules and transitions into Ms12. Consequently, QPA showed that the system consists of Ms12 (~ 54.8%), calcite (~ 1.9%), Ms10.5/Hc (~ 0.7%) and amorphous content (~ 42.6%). Additionally, it is determined that the amorphous content includes amorphous Al_2O_3 and Al_2SiO_5 , as evidenced by FTIR, STA, SEM, ^{27}Al NMR spectroscopy and mass balance calculation.

The thermal stability assessment revealed that the critical temperature for the dehydration of monosulfoaluminate is 25–370 °C. It was found that at this temperature, four different hydration states of monosulfoaluminate occur, with dehydration temperatures overlapping. Moreover, the data propose that the main interlayers' dehydration of monosulfoaluminate might begin at ~ 200 °C. Within higher temperatures (720–1250 °C), solid-state reactions are observed. The results indicate that monosulfoaluminate recrystallised into $\text{C}\bar{\text{S}}$, CA , CaO and $\text{C}_4\text{A}_3\bar{\text{S}}$. Meanwhile, the further growth of ye'elimite at 1000–1250 °C results from the solid-state reactions between $\text{C}\bar{\text{S}}$, CA and CaO . The presented results and insights enlarge knowledge of the thermal properties of monosulfoaluminate and could help to cement producers predict concrete's behaviour at high temperatures.

Data availability

The datasets generated during and/or analysed during the current study are available from the corresponding author upon reasonable request.

Received: 25 November 2022; Accepted: 3 March 2023

Published online: 07 March 2023

References

- Dorn, T., Blask, O. & Stephan, D. Acceleration of cement hydration—A review of the working mechanisms, effects on setting time, and compressive strength development of accelerating admixtures. *Constr. Build. Mater.* **323**, 126554. <https://doi.org/10.1016/j.conbuildmat.2022.126554> (2022).
- Liao, Y., Wei, X. & Li, G. Early hydration of calcium sulfoaluminate cement through electrical resistivity measurement and micro-structure investigations. *Constr. Build. Mater.* **25**, 1572–1579. <https://doi.org/10.1016/j.conbuildmat.2010.09.042> (2011).
- Padilla-encinas, P., Palomo, A., Blanco-varela, M. T. & Fernández-carrasco, L. Monitoring early hydration of calcium sulfoaluminate clinker. *Constr. Build. Mater.* **295**, 123578. <https://doi.org/10.1016/j.conbuildmat.2021.123578> (2022).
- Andrade, S., De, A. G. & Paula, A. Effects of sulfates on the hydration of Portland cement—A review. *Constr. Build. Mater.* **279**, 122428. <https://doi.org/10.1016/j.conbuildmat.2021.122428> (2021).
- García-maté, M. *et al.* Effect of calcium sulfate source on the hydration of calcium sulfoaluminate eco-cement. *Cem. Concr. Compos.* **55**, 53–61. <https://doi.org/10.1016/j.cemconcomp.2014.08.003> (2015).
- Allevi, S., Marchi, M., Scotti, F., Bertini, S. & Cosentino, C. Hydration of calcium sulfoaluminate clinker with additions of different calcium sulphate sources. *Mater. Struct. Constr.* **49**, 453–466. <https://doi.org/10.1617/s11527-014-0510-5> (2016).
- Feng, P., Miao, C. & Bullard, J. W. Factors influencing the stability of AFm and AFt in the Ca–Al–S–O–H system at 25 °C. *J. Am. Ceram. Soc.* **99**, 1031–1041. <https://doi.org/10.1111/jace.13971> (2016).
- Pöllmann, H. Syntheses, properties and solid solution of ternary lamellar calcium aluminate hydroxide salts (AFm-phases) containing SO_4 , CO_3 and OH . *Neues Jahrbuch Mineralogie—Abhandlungen* **182**, 173–181. <https://doi.org/10.1127/0077-7757/2006/0042> (2006).
- Chen, B. *et al.* Physicochemical properties of ettringite/meta-ettringite for thermal energy storage: Review. *Sol. Energy Mater. Sol. Cells* **193**, 320–334. <https://doi.org/10.1016/j.solmat.2018.12.013> (2019).
- Guimarães, D., de Oliveira, V. A. & Leão, V. A. Kinetic and thermal decomposition of ettringite synthesized from aqueous solutions. *J. Therm. Anal. Calorim.* **124**, 1679–1689. <https://doi.org/10.1007/s10973-016-5259-3> (2016).
- Shimada, Y. & Young, J. F. Thermal stability of ettringite in alkaline solutions at 80 °C. *Cem. Concr. Res.* **34**, 2261–2268. <https://doi.org/10.1016/j.cemconres.2004.04.008> (2004).
- Hartman, M. R., Brady, S. K., Berliner, R. & Conradi, M. S. The evolution of structural changes in ettringite during thermal decomposition. *J. Solid State Chem.* **179**, 1259–1272. <https://doi.org/10.1016/j.jssc.2006.01.038> (2006).
- Mishra, G., Dash, B. & Pandey, S. Layered double hydroxides: A brief review from fundamentals to application as evolving biomaterials. *Appl. Clay Sci.* **153**, 172–186. <https://doi.org/10.1016/j.clay.2017.12.021> (2018).
- Allmann, R. Refinement of the hybrid layer structure $[\text{Ca}_2\text{Al}(\text{OH})_6]^{+}[\text{1}/2\text{SO}_4\cdot 3\text{H}_2\text{O}]^{-}$. *Neues Jahrb. Für Miner. Monatshefte*, 136–143 (1977).
- Baquerizo, L. G. *et al.* Methods to determine hydration states of minerals and cement hydrates. *Cem. Concr. Res.* **65**, 85–95. <https://doi.org/10.1016/j.cemconres.2014.07.009> (2014).
- Khoshnazar, R., Beaudoin, J., Raki, L. & Alizadeh, R. Solvent exchange in sulfoaluminate phases. Part II: Monosulfate. *Adv. Cem. Res.* **25**, 314–321. <https://doi.org/10.1680/adcr.12.00042> (2013).
- Meller, N., Kyritsis, K. & Hall, C. The hydrothermal decomposition of calcium monosulfoaluminate 14-hydrate to katoite hydrogarnet and β -anhydrite: An in-situ synchrotron X-ray diffraction study. *J. Solid State Chem.* **182**, 2743–2747. <https://doi.org/10.1016/j.jssc.2009.07.029> (2009).
- Baquerizo, L. G., Matschei, T., Scrivener, K. L., Saeidpour, M. & Wadsö, L. Hydration states of AFm cement phases. *Cem. Concr. Res.* **73**, 143–157. <https://doi.org/10.1016/j.cemconres.2015.02.011> (2015).
- Pöllmann, H. *Cementitious Materials: Composition, Properties, Application* (De Gruyter, 2017). <https://doi.org/10.1515/9783110473728>.
- Cro, O. C., Leisinger, S. M., Lothenbach, B., Le, G. & Johnson, C. A. Thermodynamic modeling of solid solutions between monosulfate and monochromate $3\text{CaO}\cdot\text{Al}_2\text{O}_3\cdot\text{Ca}[(\text{CrO}_4)_x(\text{SO}_4)_{1-x}] \cdot n\text{H}_2\text{O}$. *Cem. Concr. Res.* **42**, 158–165. <https://doi.org/10.1016/j.cemconres.2011.09.005> (2012).
- Dilnesa, B. Z., Lothenbach, B., Renaudin, G., Wichser, A. & Wieland, E. Stability of monosulfate in the presence of iron. *J. Am. Ceram. Soc.* **95**, 3305–3316. <https://doi.org/10.1111/j.1551-2916.2012.05335> (2012).
- Motzet, H. & Pöllmann, H. Synthesis and characterization of sulfite-containing AFm phases in the system $\text{CaO}-\text{Al}_2\text{O}_3-\text{SO}_2-\text{H}_2\text{O}$. *Cem. Concr. Res.* **29**, 1005–1011. [https://doi.org/10.1016/S0008-8846\(99\)00082-4](https://doi.org/10.1016/S0008-8846(99)00082-4) (1999).
- Bak, S. M., Shadiké, Z., Lin, R., Yu, X. & Yang, X. Q. In situ/operando synchrotron-based X-ray techniques for lithium-ion battery research. *NPG Asia Mater.* **10**, 563–580. <https://doi.org/10.1038/s41427-018-0056-z> (2018).
- Pöllmann, H. Characterization of Different Water Contents of Ettringite and Kuzelite. *Proc. 12th Int. Congr. Chem. Cem. Monr. QC, Canada* 8–13 (2007).
- Kosenko, N. F., Belyakov, A. S. & Smirnova, M. A. Effect of mechanical activation procedure on the phase composition of gypsum. *Inorg. Mater.* **46**, 615–620. <https://doi.org/10.1134/S0020168510050195> (2010).
- Haffer, S., Weinberger, C. & Tiemann, M. Mesoporous Al_2O_3 by nanocasting: Relationship between crystallinity and mesoscopic order. *Eur. J. Inorg. Chem.* **20**, 3283–3288. <https://doi.org/10.1002/ejic.201200131> (2012).

27. Santos, P. S., Santos, H. S. & Toledo, S. P. Standard transition aluminas. Electron microscopy studies. *Mater. Res.* **3**, 104–114. <https://doi.org/10.1590/s1516-1439200000400003> (2000).
28. Damidot, D. & Glasser, F. P. Thermodynamic investigation of the CaO-Al₂O₃-CaSO₄-H₂O system at 50 °C and 85 °C. *Cem. Concr. Res.* **22**, 1179–1191 (1992).
29. Scholtzová, E., Kucková, L., Kožíšek, J. & Tunega, D. Structural and spectroscopic characterization of ettringite mineral-combined DFT and experimental study. *J. Mol. Struct.* **1100**, 215–224. <https://doi.org/10.1016/j.molstruc.2015.06.075> (2015).
30. Tambara, D. J. *et al.* Effect of alkaline salts on calcium sulfoaluminate cement hydration. *Molecules* **26**, 1–19 (2021).
31. Dietmann, K. M., Linke, T., Sánchez, M. D. N., Pavón, J. L. P. & Rives, V. Layered double hydroxides with intercalated permanganate and peroxydisulphate anions for oxidative removal of chlorinated organic solvents contaminated water. *Minerals* <https://doi.org/10.3390/min10050462> (2020).
32. Seo, J., Park, S., Kim, S., Yoon, H. N. & Lee, H. K. Local Al network and material characterization of belite-calcium sulfoaluminate (CSA) cements. *Mater. Struct. Constr.* **55**, 1–11. <https://doi.org/10.1617/s11527-021-01842-3> (2022).
33. Zhang, Y., Chang, J. & Ji, J. AH₃ phase in the hydration product system of AFt-AFm-AH₃ in calcium sulfoaluminate cements: A microstructural study. *Constr. Build. Mater.* **167**, 587–596. <https://doi.org/10.1016/j.conbuildmat.2018.02.052> (2018).
34. El Khessaimi, Y. *et al.* Solid-state synthesis of pure ye`elinite. *J. Eur. Ceram. Soc.* **38**, 3401–3411. <https://doi.org/10.1016/j.jeurceramsoc.2018.03.018> (2018).

Acknowledgements

This research was funded by a Grant (No. S-MIP21-4) from the Research Council of Lithuania.

Author contributions

This paper was written with the contribution of all authors. D.R.: investigation, methodology, validation, visualisation, writing. T.D.: data overview, validation, writing – review & editing. K.B.: conceptualisation, writing – review & editing. H.H.: performed analysis, software, and visualisation. R.S.: oversight of the experiment, supervision, and editing.

Competing interests

The authors declare no competing interests.

Additional information

Correspondence and requests for materials should be addressed to D.R.

Reprints and permissions information is available at www.nature.com/reprints.

Publisher's note Springer Nature remains neutral with regard to jurisdictional claims in published maps and institutional affiliations.



Open Access This article is licensed under a Creative Commons Attribution 4.0 International License, which permits use, sharing, adaptation, distribution and reproduction in any medium or format, as long as you give appropriate credit to the original author(s) and the source, provide a link to the Creative Commons licence, and indicate if changes were made. The images or other third party material in this article are included in the article's Creative Commons licence, unless indicated otherwise in a credit line to the material. If material is not included in the article's Creative Commons licence and your intended use is not permitted by statutory regulation or exceeds the permitted use, you will need to obtain permission directly from the copyright holder. To view a copy of this licence, visit <http://creativecommons.org/licenses/by/4.0/>.

© The Author(s) 2023